Journal of Thermal Analysis and Calorimetry, Vol. 84 (2006) 2, 367–376

# MELTING BEHAVIOUR AND EVOLVED GAS ANALYSIS OF XYLOSE

*M. Lappalainen*[1], *I. Pitkänen*[1*], *H. Heikkilä*[2] *and J. Nurmi*[2]

[1]University of Jyväskylä, Department of Chemistry, P.O. Box 35, 40014 University of Jyväskylä, Finland
[2]Danisco Sugar and Sweeteners Development Center, 02460 Kantvik, Finland

Two enantiomeric forms of xylose were identified as α-*D*-xylopyranose and α-*L*-xylopyranose by powder diffraction. Their melting behaviour was studied with conventional DSC and StepScan DSC method, the decomposition was studied with TG and evolved gases were analyzed with combined TG-FTIR technique. The measurements were performed at different heating rates. The decomposition of xylose samples took place in four steps and the main evolved gases were $H_2O$, $CO_2$ and furans. The initial temperature of TG measurements and the onset and peak temperatures of DSC measurements were moved to higher temperatures as heating rates were increased. The decomposition of *L*-xylose started at slightly higher temperatures than that of *D*-xylose and *L*-xylose melted at higher temperatures than *D*-xylose. The differences were more obvious at low heating rates. There were also differences in the melting temperatures among different samples of the same sugar. The StepScan measurements showed that the kinetic part of melting was considerable. The melting of xylose was anomalous because, besides the melting, also partial thermal decomposition and mutarotation occurred. The melting points are affected by both the method of determination and the origin and quality of samples. Melting point analysis with a standardized method appears to be a good measure of the quality of crystalline xylose. However, the melting point alone cannot be used for the identification of xylose samples in all cases.

***Keywords:*** *decomposition, DSC, EGA, melting, StepScan DSC, TG, thermal analysis, xylose*

## Introduction

One of the most common parameters to characterize materials is the melting point. It is also used for the determination of purity and for the identification of different samples. Melting is an equilibrium process under isothermal conditions but the dynamics of heating rate leads to some degree of irreversibility. Usually the melting point is determined by raising the temperature at a certain constant heating rate over the expected range of melting. This causes a temperature gradient in the sample and an apparent rise of the observed melting temperature. This is one reason why the melting proceeds over an apparent temperature range. The melting can be said to be anomalous if a change of the conformation of molecules occurs during melting. Also a decomposition taking place in the melting temperature range causes the melting to be anomalous. The anomalous melting temperature is strongly dependent on the heating rate [1].

The quality of material can also be characterized by the shape of the melting peak, usually its width. The value used for comparisons may be the peak half width or the difference of peak and onset temperatures ($T_{peak}$–$T_{onset}$). The width of peak in DSC depends on several factors, such as thermal lag, heating rate, sample size and the changes during the peak. The melting peak can also be used for determination of the purity of the sample. This well-known method is based on the equation of van't Hoff [2].

The melting of xylose has been reported in many published studies. Shafizadeh *et al.* [3, 4] found by DTA the melting point of α-*D*-xylopyranose to be 155°C while Roos [5, 6] determined the melting point of *D*-xylose with DSC. The onset and the peak values were 143 and 157°C, respectively, and the heat of fusion was 211 J $g^{-1}$. Raemy *et al.* [7] determined the fusion temperatures of *D*-xylose with heat flow calorimetry. The onset value was 135°C, the peak value 150°C and the heat of fusion 280 J $g^{-1}$. According to Lide, the melting point of α-*D*-xylose is 145°C [8]. The melting temperatures significantly differ between different references and the endotherms depicted are fairly broad.

The sugars have an ability to assume several different forms, including the open chain aldehyde or ketone and the α- and β-anomers of both five-membered (furanoid) and six-membered (pyranoid) ring structures, with each of these tautomers having a variety of possible conformations. For this reason, the stereochemistry of carbohydrates has been much studied [9, 10]. Enantiomeric relationship between the sugars is indicated with the configurational prefixes *D* and *L* that show the side (right or left, respectively) the highest numbered asymmetric carbon atom has the OH group attached in the Fischer projection formula. The anomers are expressed with prefixes α

* Author for correspondence: ipitkane@cc.jyu.fi

1388–6150/$20.00

Akadémiai Kiadó, Budapest, Hungary
Springer, Dordrecht, The Netherlands

and β and their specification is related to the configuration of the highest numbered asymmetric carbon atom. In addition, the pyranose ring can exist either as a chair-structure or as a boat-structure. The two possible pyranose chair forms are $^1C_4$ and $^4C_1$ [9–11].

Because of the stereochemistry of sugars, xylose has different crystal and molecular forms. The knowledge of crystal structure and ring conformation is important in order to understand the chemical and physical properties of sugars. The melting temperatures may differ between sugar anomers [5]. The α- and β-anomers of a sugar are at equilibrium in water, but in the crystalline state one anomer is usually the dominating form [12–14]. The percentage distribution of *D*-sugar tautomers at equilibrium in water solutions has been measured for all of the commonly occurring sugars, and in general the pyranoid rings predominate. For *D*-xylose in water at room temperature the equilibrium concentrations are approximately 65.2% for the β-pyranoid ring and 34.8% for the α-pyranoid ring, with negligible amounts of the open chain and furanoid ring forms [9, 15]. In the solid state, the crystal structure has been determined for α-*L*-xylopyranose [16–18] and for α-D-xylopyranose [19]. The conformations are $^1C_4$ for α-*L*-xylopyranose and $^4C_1$ for α-*D*-xylopyranose [9]. These sugars are depicted in Fig. 1.

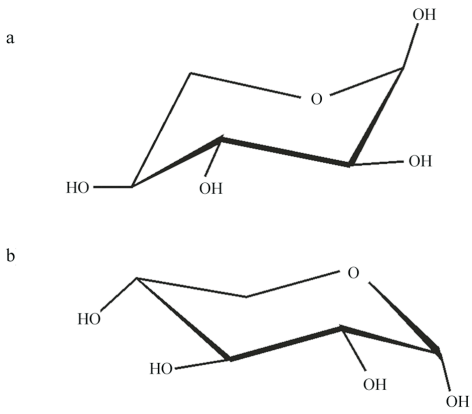


**Fig. 1** a – α-*L*-xylopyranose $^1C_4$ and b – α-*D*-xylopyranose $^4C_1$

The conformation of the sugar may change in the melting process [6].The melting endotherm of a pure organic compound is generally very sharp. According to Shafizadeh *et al.* [3, 4] the rather wide and unsymmetrical appearance of the melting peak of α-*D*-xylopyranose indicates the presence of some impurity or the occurrence of another simultaneous transformation. They also showed that the melting is accompanied by thermal anomerization of the α-*D*-xylopyranose. Upon heating, α-*D*-xylopyranose changes to β-*D*-xylopyranose. The crystalline α-*D*-anomer contains about 10% of the β-*D*-anomer up to about 125°C where the endotherm begins. It then continues to equilibrate until the melting is completed and the ratio of anomers becomes constant. At a temperature of 154°C, the ratio of α-*D*-xylopyranose and β-*D*-xylopyranose is 48:52%, respectively [3, 4].

Although xylose has been extensively discussed in literature, its melting is usually not thoroughly studied. The published values of the melting temperature of xylose differ slightly from each other and the melting range is rather broad. In addition, the form studied is not always identified and for that reason it is difficult to use the melting temperature for the identification of xylose. In this study, we have investigated the variation in the melting temperature of xylose and tried to find out how the differences could be explained. Also the values obtained for different samples using the same measurement parameters were compared with each other. Especially the decomposition was studied in a comprehensive way and also the gases evolved during TG were thoroughly analysed. The purpose of this study was to obtain more information about the processes taking place before, during and after the melting of xyloses and to explain the reasons for the broadness of the melting peak.

## Experimental

### *Materials*

Crystalline *L*-xylose (Ksyloosi erä1 22.8.2001) and *D*-xylose (Lot Z121296, >99.8%) were obtained from Danisco Sweeteners, Finland. For some additional measurements, *D*(+)-xylose (Sigmaultra 99%, Sigma-Aldrich) and *L*(–)-xylose (minimum 99%, Sigma) were used. All samples were dried over phosphorus pentoxide.

### *Methods*

The powder diffraction patterns were measured to ensure the right structural form. The X-ray powder diffraction patterns were obtained at room temperature using a Huber Imaging Plate Guinier camera G670. Germanium crystal monochromatized $CuK_{\alpha 1}$-radiation was used (λ=1.54056 Å) and the X-ray tube was operated at 45 kV and 25 mA. The samples were attached on Mylar film with vaseline. The exposure time was 30 min and the imaging plate was scanned six times. ZDS software was used to process the measurement data. The measured powder patterns were identified with the PDF-2 database of known powder diffraction patterns. Xyloses were identified as α-*L*-xylopyranose and α-*D*-xylopyranose. The crystals belong to the orthorhombic space group $P2_12_12_1$, with unit cell dimensions *a*=9.2080(4) Å, *b*=12.6067(6) Å and *c*=5.6081(2) Å (α-*L*-xylo-

pyranose) and $a$=9.1902(5) Å, $b$=12.6032(8) Å and $c$=5.6126(2) Å (α-*D*-xylopyranose). The calculated powder diffraction patterns corresponded to our measured powder diffraction patterns and no additional peaks were observed. On the basis of powder diffraction measurements, samples were considered to be of good quality and they could be easily identified.

The TG measurements were carried out on a Perkin Elmer TGA7 Thermogravimetric Analyzer using an open Pt-pan and a dynamic nitrogen atmosphere with a flow rate of 50 mL min$^{-1}$. The sample masses were 4–6 mg. The temperature range was 30–850°C and the heating rates used were 0.5, 1, 2, 10, 20 and 40 K min$^{-1}$.

The evolved gas from TG was analysed by FTIR using a measurement system consisting of Perkin Elmer TGA7 Thermogravimetric Analyser coupled to the Perkin Elmer System 2000 FTIR by transfer line. The temperature range for thermal analysis was 30–700°C, the heating rate used was 10 K min$^{-1}$ and the sample mass was 10–15 mg. The dynamic experiments were carried out both in air and nitrogen atmospheres with a flow rate of 90 mL min$^{-1}$. The temperature of the transfer line and the gas cell were adjusted to 190°C. The FTIR measurements were obtained with a resolution of 4 or 8 cm$^{-1}$ and 16 scans per slice. For the presentation of the FTIR spectra and the identification of the evolved gases, the Perkin Elmer TR-IR (time-resolved infrared spectra) of Spectrum TimeBase, Spectrum and search programs were used. The search program uses PSU (possible structure units), a select enhanced EPA vapour Phase Database (code: 4602) and the reference database of Pure Organic Compounds (code: 4050) of BIO-RAD (Sadtler). Additionally, the Socrates Infrared Characteristic Group Frequencies Tables and Charts, Second Edition of BIO-RAD, Sadtler Division, and the Aldrich Library of FTIR Spectra, Vapour Phase were used. For some individual spectra, a Spectral Database for Organic Compounds (SDBS) was consulted [20].

The melting temperatures and the heats of fusion of *L*-xylose and *D*-xylose were determined with DSC. The DSC measurements were carried out on a Perkin Elmer DSC Pyris1 instrument using 50 μL aluminium sample cups with capillary holes and a dynamic nitrogen atmosphere with a flow rate of 50 mL min$^{-1}$. The sample masses were 4–6 mg. The temperature range covered was 35–190°C, and the heating rates used (0.5, 1, 2, 10, 20 and 40 K min$^{-1}$) were the same as in TG studies. The temperature calibration was done by indium and zinc standards and the heat flow was calibrated by the melting enthalpy of the indium standard. The calibration was done with the heating rate of 2 K min$^{-1}$ and the results at different heating rates were corrected by a thermal lag of 0.058 min measured with xylitol sample, while it was 0.038 min with indium sample [21, 22]. For the slowest measurements (0.5 and 1°C min$^{-1}$) the calibration was done at the same heating rate as used in the measurements but the thermal lag correction was not used.

For comparison of different samples of the same sugar, additional measurements were done with a Pyris Diamond DSC. The temperature range was 30–170°C and the heating rate was 2 K min$^{-1}$.

The StepScan measurements were done with Pyris Diamond DSC. Two measurement parameters were used. In the first measurements, the temperature jump was 2°C, the heating rate was 2 K min$^{-1}$, the isothermal segment was 1 min and the criteria value was 0.01 mW. The values of the second measurements were 1°C, 1 K min$^{-1}$, 1 min and 0.01 mW, respectively. The temperature range was 100–170°C. The other parameters were as described above. The specific heat was calibrated by a sapphire standard.

## Results and discussion

*Thermal analysis and evolved gas analysis*

The results of the thermal analysis measurements on melting are collected in Table 1. From the TG measurements, the initial temperature of decomposition was taken as the temperature where the reduction of mass was larger than the noise in the TG curve. As can be seen in the table, the initial temperature of the TG measurements was moved to higher temperatures as heating rate increased. The decomposition of *L*-form started at higher temperatures than the decomposition of *D*-form.

**Table 1** The results of DSC and TG measurements in nitrogen. Onset and peak temperatures of melting and the heat of fusion ($\Delta H_f$) are from DSC. $T_i$ is the initial temperature of decomposition (from TG)

| Heating rate/ K min$^{-1}$ | Onset/ °C | Peak/ °C | $\Delta H_f$/ J g$^{-1}$ | $T_i$/ °C |
|---|---|---|---|---|
| *L*-xylose | | | | |
| 0.5 | 143.9 | 147.3 | 208 | 145.1 |
| 1 | 147.1 | 150.5 | 213 | 146.9 |
| 2* | 150.0 | 153.8 | 229 | – |
| 2 | 151.4 | 155.3 | 222 | 149.2 |
| 10 | 155.8 | 160.8 | 237 | 164.6 |
| 20 | 159.2 | 164.8 | 240 | 187.5 |
| 40 | 162.2 | 168.4 | 251 | 198.0 |
| *D*-xylose | | | | |
| 0.5 | 136.8 | 142.4 | 207 | 138.5 |
| 1 | 139.7 | 145.8 | 216 | 147.0 |
| 2* | 142.6 | 149.6 | 217 | – |
| 2 | 143.7 | 150.1 | 222 | 147.1 |
| 10 | 152.8 | 157.7 | 228 | 160.7 |
| 20 | 156.3 | 162.7 | 236 | 174.0 |
| 40 | 158.3 | 166.3 | 239 | 184.4 |

*non-dried sample

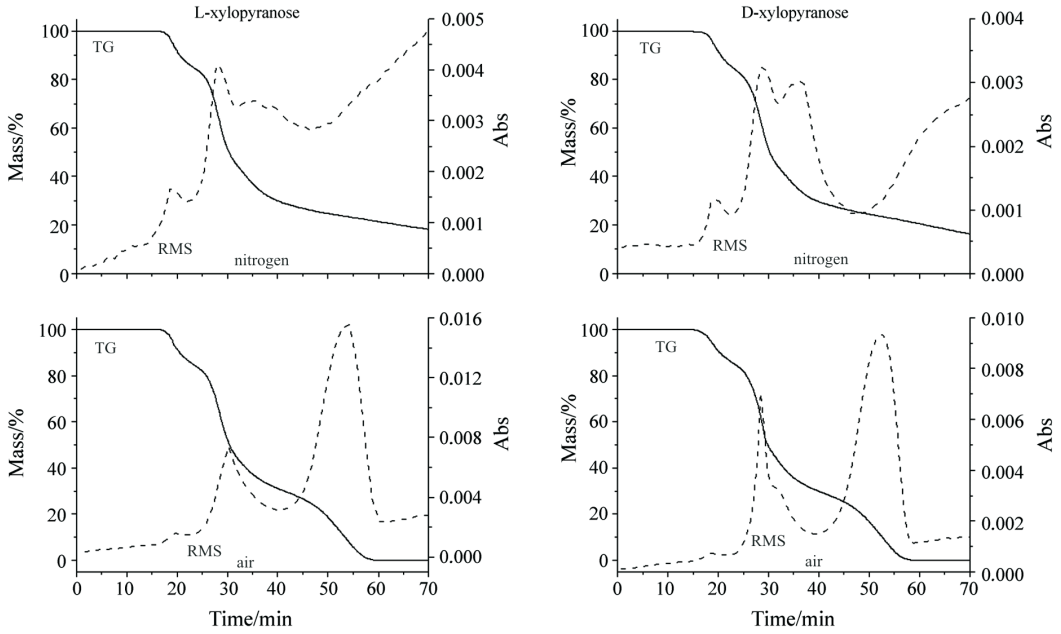


**Fig. 2** — – TG curves and --- – RMS intensity profiles of *L*- and *D*-xylose measured in air and nitrogen at a heating rate of 10 K min$^{-1}$

The pyrolysis experiments were described in our earlier paper [23]. The main decomposition products of the pyrolysis of *D*-xylose were (2H)-furan-3-one, 2-furancarboxaldehyde, furanmethanol, 1-(2-furanyl)-ethanone, α-angelicalactone, 3-hydroxy-2-penteno-1,5-lactone, 3-methyl-1,2-cyclopentanedione, methyl ester of furoic acid, 1,6-anhydro-β-*D*-glucopyranose and hexadecanoic acid. $CO_2$, $H_2O$ and other light compounds were not determined because the mass range of the mass spectrometer was 45–300.

The decomposition took place in four steps according to TG. The mass losses are shown in Table 2. The detected peaks of the RMS (=root-mean-square) intensity profiles of the total evolved gases used in the FTIR experiments paralleled the TG curves very well, as shown in Fig. 2. The peak values of DTG and RMS curves are shown in Table 3. Figure 3 presents the stacked plot diagrams of α-*D*-xylopyranose in air and in nitrogen while Fig. 4 presents gas spectra of *D*-xylose at 19.4, 28.7 and 48.0 min (224, 317 and 510°C, respectively) in nitrogen.

**Table 2** Mass loss/% of *D*- and *L*-xyloses in the heating rates of 2 and 10 K min$^{-1}$ in air and nitrogen from TG measurements. Starting temperature was 30°C in all measurements. The time range column included relates to the evolved gas analysis measurements that were done only at a heating rate of 10 K min$^{-1}$

| Atmosphere | 2 K min$^{-1}$ | | 10 K min$^{-1}$ | | |
|---|---|---|---|---|---|
| | $T_{range}$/°C | mass loss/% | $T_{range}$/°C | $t_{range}$/min | mass loss/% |
| *L*-xylose | | | | | |
| air | 140–234 | 17.8 | 158–247 | 12.8–21.7 | 15.1 |
| | 234–300 | 28.3 | 247–339 | 21.7–30.9 | 41.9 |
| | 300–392 | 20.5 | 339–426 | 30.9–39.6 | 12.7 |
| | 392–537 | 33.9 | 426–622 | 39.6–59.2 | 30.2 |
| nitrogen | 157–247 | 17.4 | 161–248 | 13.1–21.8 | 14.9 |
| | 247–320 | 31.5 | 248–344 | 21.8–31.4 | 43.1 |
| | 320–424 | 17.0 | 344–517 | 31.4–48.7 | 17.2 |
| | 424–731 | 11.3 | 517–850 | 48.7–82.0 | 10.4[a] |
| *D*-xylose | | | | | |
| air | 149–228 | 17.0 | 156–246 | 12.6–21.6 | 14.8 |
| | 228–317 | 34.2 | 246–331 | 21.6–30.1 | 41.0 |
| | 317–390 | 13.3 | 331–412 | 30.1–38.2 | 14.1 |
| | 390–526 | 35.8 | 412–618 | 38.2–58.8 | 30.2 |
| nitrogen | 148–244 | 17.1 | 152–242 | 12.1–21.2 | 14.6 |
| | 244–323 | 33.7 | 242–344 | 21.2–31.4 | 44.1 |
| | 323–425 | 17.0 | 344–521 | 31.4–49.1 | 17.1 |
| | 425–750 | 13.9 | 521–850 | 49.1–82.0 | 13.2[b] |

Residuals in nitrogen: [a]14.4%, [b]11.1%

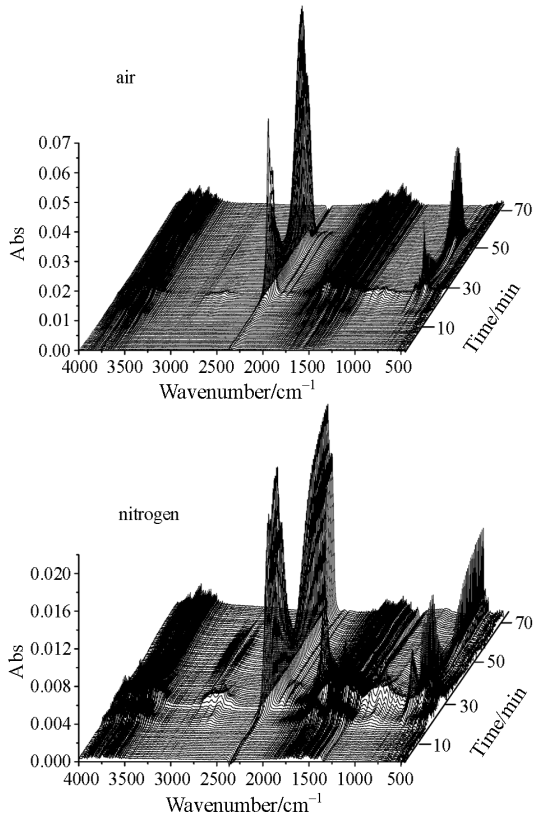


**Fig. 3** Stacked plot pictures of *D*-xylose in air and nitrogen

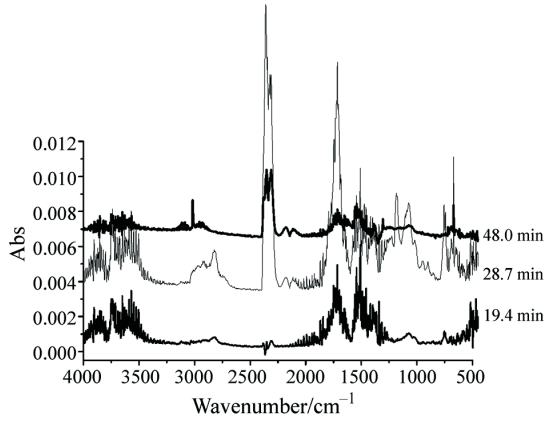


**Fig. 4** FTIR spectra of evolved gas products of xylose in nitrogen

The first steps were nearly the same both in air and nitrogen atmospheres. In all cases, the decomposition started when a major part of xylose melted when heated at a rate of 10 K min$^{-1}$. The fastest mass decrease in the first step took place at 207–218°C, as judged on the basis of the DTG curves. Ohnishi *et al.* [24, 25] observed for the some material a DTG peak temperature of 210°C in helium purge gas. On the basis of stack plot figures and separated gas spectra, $H_2O$ and furans were the main decomposition gases. 2-furaldehyde was the furan most abundant. Main peaks in the IR spectrum of 2-furaldehyde are 2810 (m, broad), 1718 (vs), 1574 (m), 1478 (m), 1015 (m) and 755 (s), where vs, s and m refer to very strong, strong and medium peak intensity, respectively. It was also an abundant degradation compound in pyrolysis [23]. According to Köll *et al.* [26] and Domburgs and Sergeeva [27] also 1,5-anhydropentofuranose and 1,4-anhydropentopyranoses [28] were formed, and forming of these produces water. They themselves do not evaporate at these temperatures. Köll *et al.* [26] observed in vacuum pyrolysis of *D*-xylose 5% 1,5-anhydro-β-*D*-xylofuranose among the degradation products. $CO_2$ started to form during the latter part of the first step. The initial stage of heat treatment of xylose was characterized by processes of its anhydridization (dehydration, caramelization) and polymerization. Increasing the temperature above 200°C led to depolymerization and breakdown products of *D*-xylose and *D*-xylose polymers [3, 4, 29].

The heating rate influenced the mass loss as measured by the TG curve. This can be seen in Table 2, where mass loss at the heating rate of 2 K min$^{-1}$ was about 17%, while it was about 15% at the heating rate of 10 K min$^{-1}$. This is analogous to the pyrolysis results of Domburgs and Sergeeva, where the amount of 2-furaldehyde (2-furancarboxaldehyde) increased as a function of pyrolysis time [27].

**Table 3** The temperature of peaks of DTG- and RMS-curves in *D*-xylose and *L*-xylose measured in air and nitrogen. Starting temperature was 30°C and heating rate 10°C min$^{-1}$. The peak values are presented in both minutes and degrees

| | *D*-xylose | | | | *L*-xylose | | | |
|---|---|---|---|---|---|---|---|---|
| | air | | nitrogen | | air | | nitrogen | |
| | time/min | temperature/°C | time/min | temperature/°C | time/min | temperature/°C | time/min | temperature/°C |
| DTG | 18.6 | 216 | 18.7 | 217 | 18.9 | 219 | 18.7 | 217 |
| | 28.7 | 317 | 28.5 | 315 | 28.4 | 314 | 28.2 | 312 |
| | 30.9 | 339 | 33.6 | 366 | 31.9 | 349 | 33.4 | 364 |
| | 52.5 | 555 | 61.2 | 642 | 52.6 | 556 | 61.7 | 647 |
| RMS | 18.7 | 217 | 19.5 | 225 | 19.8 | 228 | 18.8 | 218 |
| | 28.4 | 314 | 28.8 | 318 | 30.2* | 332* | 28.0 | 310 |
| | 31.1 | 341 | 34.7 | 377 | – | – | 35.1 | 381 |
| | 52.6 | 556 | >60 | >630 | 53.5 | 565 | >60 | >630 |

*The second and third peaks were not resolved

During the second degradation step the temperature of the fastest decomposition changed very little in all measured cases. However, mass losses in TG curves were larger at faster heating rate. Partly, this arises from the different amounts of 2-furaldehyde formed. Also the separation of the second and third step from each other was difficult already at the heating rate of 10 K $min^{-1}$ in air. Although mass losses were nearly the same in nitrogen and air, the amount of $CO_2$ was about three times larger in air than in nitrogen, while the amount of water did not change appreciably between the air and nitrogen atmospheres at the heating rate of 10 K $min^{-1}$. This means that furans and other degradation compounds partly burned in air to form $CO_2$. The FTIR-spectra of $H_2O$ and $CO_2$ were so dominant in air that it was difficult to separate other compounds, except 2-furaldehyde. The situation was totally different in nitrogen. Although in nitrogen the main decomposition compounds were $CO_2$ and $H_2O$, it was easy to recognise 2-furaldehyde, 2-furanmethanol (furfuryl alcohol), 2-acetylfuran (1-(2-fyranyl)-ethanone), 5-methyl-2(3H)furanone (alpha-angelica lactone) and methyl 2-furoate. 3-methyl-1,2-cyclopentanedione has one very strong peak at 1650 $cm^{-1}$ and other much weaker ones. Unfortunately one peak of water vapour is situated at 1651 $cm^{-1}$. In the third and fourth step this peak increased compared to the other peaks of water vapour. The second strongest peak of 3-methyl-1,2-cyclopentadiene is observed at 724 $cm^{-1}$. $CO_2$ has a peak at 719.9 $cm^{-1}$. In experimental spectra a peak was observed between 718–722 $cm^{-1}$ and in some spectra a weak peak was seen at 724 $cm^{-1}$. In addition, 3-hydroxy-2-penteno-1,5-lactone (5,6-dihydro-4-hydroxy-2H-pyran-2-one), which has a high boiling point, and (2H)-furan-3-one (3(2H)-furanone) were found in our earlier pyrolysis study [23]. We did not obtain FTIR gas spectra of these; however, these compounds may be considered possible but not confirmed on the basis of PSU.

The temperature range of the third step was 330–430°C in air and 340–520°C in nitrogen. The main decomposition gases were $CO_2$ and $H_2O$ in both cases. Furanes, other carbonyl compounds and CO were found only as minor products. Methane (main peaks at 3016 and 1304 $cm^{-1}$) was found as a new compound in nitrogen. It was formed also during the fourth step until 680°C.

The organic residues burn into $CO_2$ in air and $H_2O$ and CO could be recognised in the fourth step. The black carbon containing tar not burned in nitrogen but remained in amounts from 10 to 14 mass% at the heating rate of 10 K $min^{-1}$. The decomposition of α-*L*-xylopyranose did not differ from α-*D*-xylopyranose within the experimental uncertainty between different measurements. 1,6-anhydro-β-*D*-glucopyranose (levoglucosan) was confirmed as a degradation compound in our earlier pyrolysis measurement [23]. In TG-FTIR it could be found only to a minor extent. According to Heyns and Klier [30], this and many other degradation compounds are possibly formed via a polymeric intermediate, which then undergoes secondary thermal degradation. Levoglucosan is possibly formed during the first step but it evaporates at a much higher temperature (melting point 180–181°C, boiling point 383±42°C).

To help understand the degradation processes and formation of gaseous compounds we can draw some simplified conclusions from the above results. In a melt of xyloses, α- and β-xylopyranose are at equilibrium with α- and β-xylofuranose. The change from pyranose to furanose is possible during ring-opening. Angyal and Pickles [31] have studied the different forms at equilibrium in a deuterium oxide solution. 2-furaldehyde, 2-furanmethanol, 5-methyl-2(3H)-furanone and (2H)-furan-3-one can be formed by splitting off groups from furanose and reorganisation of bonds, as presented in Fig. 5. The situation in methyl-2-furoate and 2-acetylfuran is complicated because an addition reaction is also needed. 3-hydroxy-2-penteno-1,5-lactone, possibly formed from pyranose structure, and formation of 3-methyl-1,2-cyclopentanedione assume opening of pyranose ring and new closing. This kind of mechanism may also be possible in the compounds mentioned above.

### *The melting temperature dependence of heating rate*

The results of the DSC measurements are collected in Table 1. As can be seen in the table, increasing the heating rate causes the onset and peak temperatures to move higher and the peaks to become slightly broader. The enthalpy of melting increased as the heating rate increased.

There were differences between the *L*- and *D*-forms. The *L*-form melted at higher temperatures than the *D*-form. The temperatures differed substantially at low heating rates of 0.5 to 2 K $min^{-1}$ (7°C for onsets and 5°C for peaks), but less (2–4°C) at higher heating rates. The temperatures were overall higher for the *L*-form than for the *D*-form. In both samples studied, the shape of peaks was normal but the peaks of *D*-form were in general broader than those of *L*-form. The enthalpy of melting of both samples was nearly equal at slow heating rates but was a little higher for *L*-form than *D*-form when higher heating rates were used. When comparing our TG values with the melting values by DSC it was obvious that decomposition of both enantiomeric forms of xylose began at slow heating rates before the melting ended. At high heating rates the melting clearly occurred before the decomposition started.

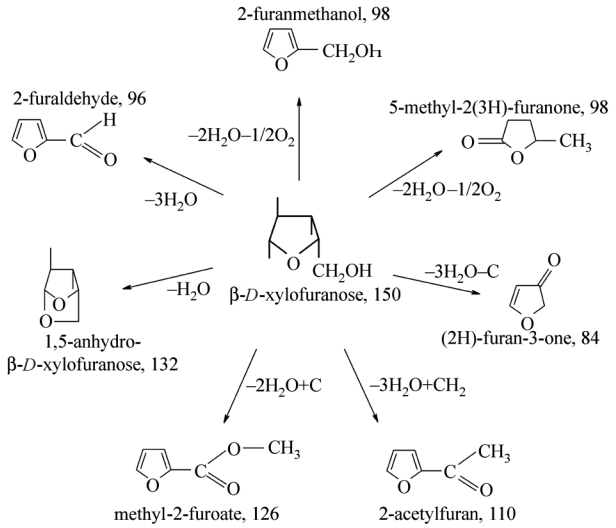


**Fig. 5** Decomposition products of β-*D*-xylofuranose

Measurements were mainly done using $P_2O_5$ dried samples. For comparison, a couple of measurements were done without drying the sample just before measurements. When measurements of $P_2O_5$ dried and non-dried samples were compared, it was noticed that the $P_2O_5$ drying moved both the onset and peak temperatures slightly to higher temperatures for both *L*- and *D*-forms but the peak width remained unchanged.

The results of this study can be compared with the data published earlier. The reported melting range of *D*-xylose is 145–157°C [3–8]. Our values at different heating rates are comparable with those results: for example the peak value of a heating rate of 2 K min$^{-1}$ was 150°C and at a heating rate of 10 K min$^{-1}$ it was 157.9°C. The peaks were narrower in this study. Roos [5, 6] and Raemy [7] observed a peak-onset difference of *D*-xylose of 14 and 15°C, respectively; our values were clearly lower (<8°C) at all heating rates. For comparison, the peak-onset difference of xylitol was 1.2°C at heating rate of 2 K min$^{-1}$ as sample mass was 6 mg.

In thermodynamic melting, the onset temperature should not change although the heating rate changes, expect for the amount of thermal lag. Thermal lag depends on numerous factors, such as the capability of the instrument to change energy during heating, the response time of the instrument, the heat conduction from the heater to the pan and further to the sample, and the heat capacity and enthalpy of melting of the sample. Instead of indium, the thermal lag was measured with xylitol because its melting is normal but the heat conductivity and specific heat are more similar than those of xyloses. In normal melting the thermal lag of onset temperature is linearly proportional to the heating rate. At slow heating rates the change of onset temperature was larger than at high heating rates (Table 1). The melting of xylose was anomalous at slow heating rates because, besides the melting, also partial thermal decomposition and mutarotation occurred. At higher heating rates, judged from the TG data, the mutarotation was the predominant factor in the change of the melting point.

### *The melting temperature dependence of different samples*

In order to compare the possible differences in samples produced by different manufacturers, two samples of both the *L*- and *D*-xylose were measured by DSC. These measurements were all done at a heating rate of 2 K min$^{-1}$. The onset and peak temperatures were calculated. In addition, the purity of a sample was determined by fitting a portion of a DSC curve to the Van't Hoff relationship. The results are given in Table 4.

There were noticeable differences among the samples of the same sugar. The onset and peak values of different *L*-xylose samples varied substantially, whereas the values of *D*-xylose samples were more in agreement with each other. The melting enthalpies were similar for all samples. The purity values varied slightly between different samples and were lower than the values of chemical purity given by the manufacturers. The reason might be that the purity values were calculated from melting peaks even thought the melting was not a pure thermodynamic equilibrium melting process.

### *StepScan measurements*

The StepScan DSC is temperature modulated DSC software by PerkinElmer Instruments for enhanced

**Table 4** The comparison of different samples. All measurements were done at a heating rate of 2°C min$^{-1}$

| | Onset/°C | Peak/°C | $\Delta H$/J g$^{-1}$ | Purity/% | $\Delta H$*/kJ mol$^{-1}$ | $\Delta H$*/J g$^{-1}$ |
|---|---|---|---|---|---|---|
| *L*-xylose | | | | | | |
| sample1 | 151.4 | 155.3 | 222 | 97.6 | 38.3 | 255 |
| sample2 | 149.3 | 150.4 | 223 | 96.5 | 39.0 | 260 |
| *D*-xylose | | | | | | |
| sample1 | 143.7 | 150.1 | 222 | 95.6 | 40.8 | 272 |
| sample2 | 145.9 | 151.3 | 226 | 97.0 | 39.8 | 265 |

*A corrected melting enthalpy to 100% purity

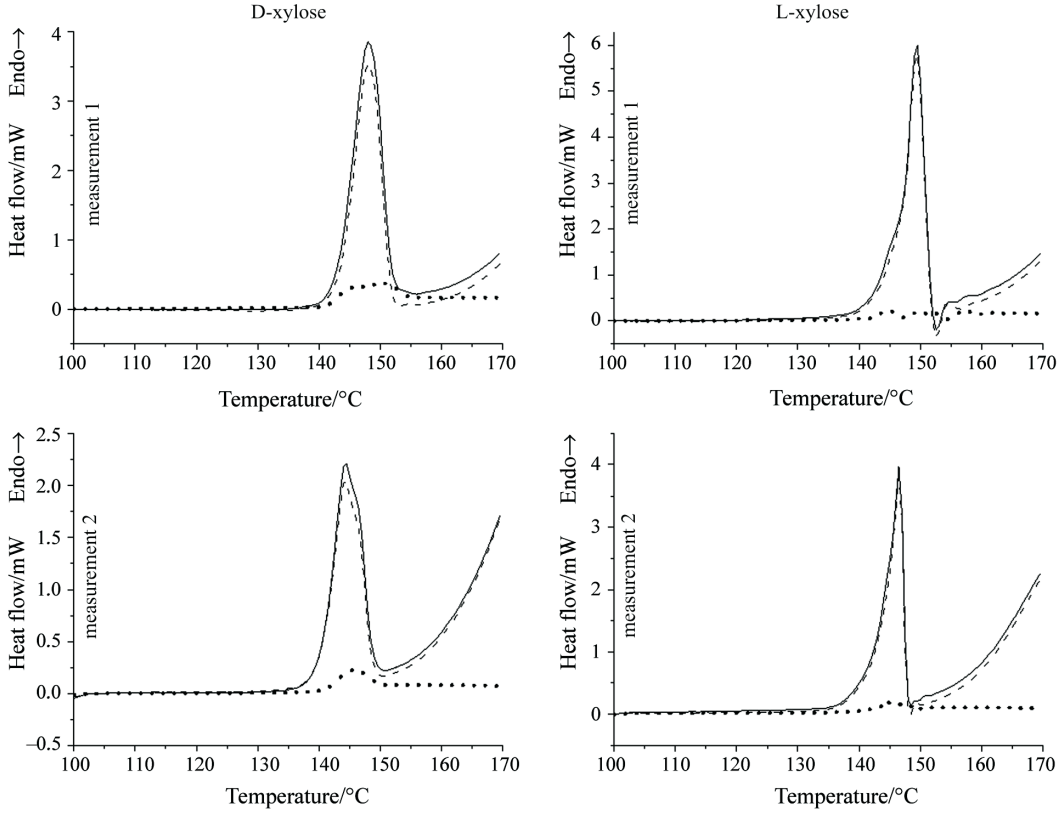


**Fig. 6** StepScan measurements. — – total heat flows, --- – kinetic part of heat flow curve ··· – thermodynamic part of heat flow curve

characterization of the thermal properties of materials. The technique permits the separation of DSC results into thermodynamic (reversible) and kinetic (non-reversible) components for better interpretation. StepScan produces a temperature program that consists of a series of short heating and isothermal steps. The basic equation describing the heat flow response from a StepScan DSC experiment is given as: $dQ/dt=C_p(dT/dt)+K(T,t)$. In this equation $dQ/dt$ is the DSC heat flow, $C_p$ is the sample's heat capacity, $dT/dt$ is the applied heating rate and $K(T,t)$ is the temperature and time depending kinetic component [32–40].

Two measurements with different measurement parameters were performed for both *L*- and *D*-xylose samples. The results of StepScan measurements are illustrated in Fig. 6. For better comparison between the different curves, both kinetic and thermodynamic curves were converted to heat flow curves. The kinetic heat flow was a straight IsoK baseline curve while the thermodynamic heat flow was calculated from thermodynamic $C_p$ curve and the total heat flow was obtained by adding together the kinetic and thermodynamic heat flow curves. At the melting temperature, the change was seen in both thermodynamic and kinetic curves.

Melting is an equilibrium process where the solid and liquid are in thermodynamic equilibrium at constant temperature and pressure. If the pseudo-isothermal temperature modulated heating technique is used for the determination of melting the situation corresponds isothermal melting. In the temperature modulated system, for example StepScan DSC, when slow overall heating rate is used, the melting is nearly an isothermal process in case of normal melting. In anomalous melting, a change of conformation of molecules occurs or decomposition takes place during melting. Anomalous melting temperature is strongly dependent on the rate of heating.

The peaks of kinetic IsoK baseline curves indicated that melting was not only a thermodynamic equilibrium process. The peak of IsoK baseline curve was calculated (Table 5). There were differences be-

**Table 5** The StepScan measurements. The isothermal segment was 1 min and the criteria was 0.01 mW in all measurements

| | | Temp. jump/°C | Heating rate/K min$^{-1}$ | Onset/°C | Peak/°C | $\Delta H$/J g$^{-1}$ |
|---|---|---|---|---|---|---|
| *L*-xylose | m1 | 2 | 2 | 145.9 | 149.4 | 217.3 |
| | m2 | 1 | 1 | 143.1 | 146.6 | 216.0 |
| *D*-xylose | m1 | 2 | 2 | 143.0 | 148.0 | 207.9 |
| | m2 | 1 | 1 | 140.4 | 144.2 | 209.0 |

tween *D*- and *L*-xylose and also between different measurements of the same sample. The slower overall heating rate of the second measurements gave a slightly lower onset and peak temperatures for the second measurements than the first measurements of both samples. The melting enthalpies were similar for both measurements and the values of *L*-xylose were higher than those of *D*-xylose. The onset and peak temperatures were slightly lower than the values obtained in conventional DSC (Tables 1 and 4). The melting enthalpies were also somewhat lower. However, the melting enthalpies calculated from the kinetic IsoK baseline curves were only a little smaller than the enthalpies obtained by conventional DSC. This shows the considerable kinetic component in the melting in these measurements.

## Conclusions

The behaviour of xylose is typical for sugars in which fairly broad melting endotherms occur over the melting temperature range. The melting of xylose is accompanied by thermal mutarotation of equilibration of α- and β-xylopyranose with α- and β-xylofuranose forms, which results in a broadening of the melting point endotherm.

The decomposition of xyloses took place in four steps according to TG. The initial temperature of TG mass loss was moved to higher temperatures as heating rates increased. $H_2O$, $CO_2$ and furans were the main decomposition gases. The heating rate influenced the mass loss in the TG curve.

The decomposition of *L*-xylose started at higher temperatures than that of *D*-xylose. *L*-xylose also melted at higher temperatures than *D*-xylose and their thermal behaviour differed especially at low heating rates. There were also differences in melting temperatures among the different samples of the same sugar. At slow heating rates the decomposition began before melting ended. At high heating rates the melting clearly occurred before the decomposition started. The StepScan measurements confirmed that melting was not only a thermodynamic equilibirium process. The melting enthalpies calculated from the kinetic curves were only a little smaller than the enthalpies obtained by conventional DSC that showed how considerable the kinetic part of melting was. The melting of xylose was anomalous because, besides the melting, also partial thermal decomposition and mutarotation occurred.

The results of melting points confirmed that the melting point determinations are affected by both the method of determination and the origin and quality of samples. The melting point is a good measure for quality analysis but it cannot be used alone in all cases for the identification of xylose samples.

## Acknowledgements

Financial support from the Research Foundation of Orion Corporation and from the City of Kotka is gratefully acknowledged.

## References

1 M. Hurtta, I. Pitkänen and J. Knuutinen, Carbohydr. Res., 339 (2004) 2267.
2 J. L. McNaughton and C. T. Mortimer, Differential Scanning Calorimetry, reprinted from 'IRS; Physical Chemistry Series 2, Volume 10', The Perkin-Elmer Corporation, Connecticut 1975, pp. 24–28.
3 F. Shafizadeh, G. D. McGinnis, R. A. Susott and H. W. Tatton, J. Org. Chem., 36 (1971) 2813.
4 F. Shafizadeh, J. Polym. Sci.: Part C, 36 (1971) 21.
5 Y. Roos, Phase Transitions in Foods, Academic Press Inc., San Diego 1995.
6 Y. Roos, Carbohydr. Res., 238 (1993) 39.
7 A. Raemy and T. F. Schweizer, J. Thermal Anal., 28 (1983) 95.
8 D. R. Lide, CRC Handbook of Chemistry and Physics, 74th Ed. CRC Press, Boca Raton 1993.
9 R. S. Shallenberger, Advanced Sugar Chemistry, The Avi Publishing Company Inc., Westport, Connecticut 1982.
10 J. F. Stoddart, Stereochemistry of Carbohydrates, Wiley-Interscience, New York 1971.
11 R. S. Shallenberger and G. G. Birch, Sugar Chemistry, The Avi Publishing Company Inc., Westport, Connecticut 1975.
12 R. Polacek, J. Stenger and U. Kaatze, J. Chem. Phys., 116 (2002) 2973.
13 R. K. Schmidt, M. Karplus and J. W. Brady, J. Am. Chem. Soc., 118 (1996) 541.
14 Q. Liu and J. W. Brady, J. Am. Chem. Soc., 118 (1996) 12276.
15 J. Angyal, Aust. J. Chem., 21 (1968) 2737.
16 S. Takagi and G. A. Jeffrey, Acta Cryst., B35 (1979) 1482.
17 A. Hordvik, Acta Chem. Scand., 25 (1971) 2175.
18 G. A. Jeffrey and A. Robbins, Acta Cryst., B36 (1980) 373.
19 N. Zaman, J. Bangladesh Acad. Sci., 10 (1986) 177.
20 http://www.aist.go.jp/RIODB/SDBS/menu-e.html
21 M. Hurtta and I. Pitkänen, Thermochim. Acta, 419 (2004) 19.
22 T. F. Pijpers, V. B. F. Mathot, B. Goderis, R. L. Scherrenberg and E. W. van der Vegte, Macromolecules, 35 (2002) 3601.
23 U. Räisänen, I. Pitkänen, H. Halttunen and M. Hurtta, J. Therm. Anal. Cal., 72 (2003) 481.
24 A. Ohnishi, K. Katõ and E. Takagi, Carbohydr. Res., 58 (1977) 387.
25 A. Ohnishi, E. Takagi and K. Katõ, Carbohydr. Res., 50 (1976) 275.
26 P. Köll, S. Deyhim and K. Heyns, Chem. Ber., 106 (1973) 3565.
27 G. Domburgs and V. N. Sergeeva, Latvijas PSR Zinatnu Akademijas Vestis, 5 (1960) 109.
28 M. Hori and F. Nakatsubo, Carbohydr. Res., 309 (1998) 281.
29 G. Dombrugs, O. I. Zil'berbrand, V. I. Kasatochkin and V. N. Sergeeva, Latvijas PSR Zinatnu Akademijas Vestis Kimijas Serija, (1962), pp. 299–303.
30 K. Heyns and M. Klier, Carbohydr. Res., 6 (1968) 436.

31 S. J. Angyal and V. A. Pickles, Aust. J. Chem., 25 (1972) 1695.
32 M. Merzlyakov and C. Schick, Thermochim. Acta, 380 (2001) 5.
33 W. J. Sichina and R. B. Cassel, Proceedings of the NATAS Annual Conference on Thermal Analysis and Applications, 28 (2000) 158.
34 B. Cassel, Am. Lab., 32 (2000) 23.
35 W. J. Sichina, Am. Lab., 33 (2001) pp. 16, 18–20, 22–26.
36 K. Pielichowski, K. Flejtuch and J. Pielichowski, Polymer, 45 (2004) 1235.
37 M. Sandor, N. A. Bailey and E. Mathiowitz, Polymer, 43 (2002) 279.
38 K. Pielichowski and K. Flejtuch, Polimeri, 49 (2004) 558.
39 B. Cassel, P. Scotto and B. Sichina, Proceedings of the NATAS Annual Conference on Thermal Analysis and Applications, 27 (1999) 33.
40 P. Robinson, Medical Plastics, 15 (2001) 114.

Received: October 15, 2005
Accepted: October 25, 2005

DOI: 10.1007/s10973-005-7400-6